Frontiers in Heat and Mass Transfer (FHMT), 18, 29 (2022)
DOI: 10.5098/hmt.18.29

Global Digital Central
ISSN: 2151-8629

Frontiers in Heat and Mass Transfer

Available at www.ThermalFluidsCentral.org

EFFECT OF RIB HEIGHT ON HEAT TRANSFER ENHANCEMENT BY COMBINATION OF A RIB AND PULSATING FLOW

Shintaro Hayakawa[a], Takashi Fukue[a*,†], Yasuhiro Sugimoto[a], Wakana Hiratsuka[b], Hidemi Shirakawa[c], Yasushi Koito[d]

[a] *Kanazawa Institute of Technology, Ishikawa 921-8501, Japan*
[b] *Former student, Iwate University, Iwate 020-8551, Japan*
[c] *National Institute of Technology, Toyama College, Toyama 939-8630, Japan*
[d] *Kumamoto University, Kumamoto 860-8555, Japan*

ABSTRACT

This paper describes the effects of a combination of rib and pulsating flow on heat transfer enhancement in an mm-scale model that simulates the narrow flow passages in cooling devices of downsized electronic equipment. This research aims to develop a novel water cooling device that increases heat transfer performance while inhibiting pumping power. Our recent study has reported that a combination of pulsating flow and rib could enhance heat transfer performance relative to the simple duct. In the present study, to verify the optimal rib height for improving heat transfer by pulsating flow, we evaluated the relationship between heat transfer performance of pulsating flow and rib height through three-dimensional computational fluid dynamics (CFD) analysis. The cooling performance index η was calculated to evaluate the improvement of the heat transfer performance of pulsating flow relative to a steady flow. Higher height ribs help to achieve higher heat transfer performance regardless of the flow pulsation. However, pressure drop also increases significantly, and the level of the heat transfer enhancement by the higher ribs is dependent on the time-averaged Reynolds number. By evaluating the cooling performance index, we clarified the optimum rib height that can enhance heat transfer while inhibiting the increase of the pressure drop.

Keywords: *CFD Analysis, Cooling Performance Index, Pulsating Flow, Rib, Thermal Design of Electronic Equipment, Water Cooling Device*

1. INTRODUCTION

Today's electronic devices have high-performance features that meet the various needs of users. Electronic equipment has also been downsized to meet miniaturization needs. Advanced cooling design methods and techniques of miniaturized electronic equipment are strongly demanded (Velardo et al., 2021). One example is power devices for inverters. Inverters control motors' rotation speed by converting direct current power from batteries to alternating current power at an arbitrary frequency and a random current. Inverters play a crucial role in electric vehicles (EVs). From saving energy, the share of EVs in the global market is expected to grow significantly. The role of inverters is expected to diversify more than ever. It is a fact that some countries have already decided to forbid sales of new gasoline cars and diesel cars in the near future to create a sustainable society.

In such a global EV shift, EVs must have higher vehicle performance, longer driving distance, and downsizing to enhance the mountability on a vehicle. However, the high performance of EV electronic drive systems also increases heat dissipation and power consumption. In addition, the thermal management of products becomes extremely complicated due to the downsized body's dimensional restrictions of the cooling device. This issue is common to not only EVs but also other electronic devices. In order to maintain the operation of electronic devices, it is necessary to achieve efficient cooling so that the mounted components inside the devices do not exceed the operation guarantee temperature. Thermal management of electric vehicles is one of the trend problems of heat transfer design in applications. For example, Singh et al., 2021 have reported an investigation of thermal management of the electric vehicle battery system.

Water cooling devices are widely used for heat dissipation from electronic devices such as power devices and processors, which have high dissipation density and are difficult to cool by forced air convection cooling. Methods to improve water cooling performance include increasing the flow rate of the water, increasing the heat transfer area such as a heat sink (e.g., Yabo et al., 2019), and mounting turbulence promoters, such as ribs (e.g., Yang et al., 2018) and vortex generators (e.g., Bons et al., 2000, Boonloi et al., 2022). In particular, the rib array is widely used in narrow flow passages to enhance heat transfer. However, high-performance pumps are needed in these techniques because these techniques generate high-pressure drops. High-performance pumps also produce more noise and consume more power. A new cooling method that features power-saving and improved cooling performance should be developed for the above reasons.

This study aims to develop a novel cooling device that can achieve high cooling performance in high-density packaging electronic equipment. Pulsating flow is observed in blood flow in the living body. If all the blood vessels in the human body are lined up end to end, the total length could wrap around Earth more than two times. Sakai (2010) disclosed that the blood transport system could perform long-distance blood transport quickly. This blood transport is achieved by the heart's pumping system, which generates pulsating flow, one of the remarkable flow characteristics of the human body. Such flow pulsation phenomena as blood flow have been confirmed in nature. The existence of flow

† *Corresponding author. Email: fukue@neptune.kanazawa-it.ac.jp*

Global Digital Central
ISSN: 2151-8629

pulsation may have some beneficial effects on flow systems. It was reported that pulsating flow could be used as a novel cooling method in fan-cooled electronic equipment. Fukue et al. (2014) evaluated the effectiveness of pulsating airflow for cooling high-density packaging electronic equipment and investigated heat transfer performance around a cylindrical obstruction experimentally, which simulated an electronic component. They found that the cooling performance of the pulsating airflow, in which the time-averaged supply flow rate of cooling air was lower than the steady airflow, was almost the same as that of the steady airflow. The pulsating flow showed some beneficial effects for cooling electronic equipment. We set our sights on applying pulsating flow in a next-generation cooling system with the high cooling performance from these backgrounds.

We focused on a combination of a rib and pulsating flow. Our recent study (Hiratsuka et al., 2020) showed that the combination of pulsating flow and the rib enhanced heat transfer performance against the combination of steady flow and the simple duct. However, we were unable to investigate the design information of rib dimensions to optimize the heat transfer performance of the combination of pulsating flow and rib. Some researchers have recently reported about the pulsating flow and the ribs. For instance, Davletshin et al. (2020) have clarified the pulsating flow's heat transfer and flow patterns around a single rib through the experiment. Yang et al. (2018) have investigated the heat transfer performance in the ribbed channels while changing the installed angle of the ribs. However, these researches investigated the heat transfer of the ribbed channel under higher Reynolds number conditions, that the flow condition was turbulent flow. In addition, these previous researches investigated the ribbed channels that there are enough clearance between the top of the ribs and the celling of the flow passage. In the miniaturized cooling devices for electronic devices, the dimensions of the coolant passage is generally restricted. Therefore the clearance around the rib becomes narrow. Moreover, the higher flow rate cannot be supplied and the optimum heat transfer enhancement method under laminar flow conditions has to be investigated. Therefore, to develop an optimum heat transfer enhancement method for narrow flow passage in the cooling devices of miniaturized electronic equipment, more detailed information of heat transfer and flow performance of the pulsating flow and the rib should be obtained under narrow flow passage and laminar flow conditions.

In this study, we investigated the relationship between the heat transfer performance of the pulsating flow and the height of a rib mounted in a mini-channel, which simulates flow passage in a water-cooled mini-channel. We conducted three-dimensional computational fluid dynamics (CFD) analysis to clarify the relationship between the heat transfer enhancement by the pulsating flow and the rib height to optimize the pulsating flow's enhancement.

2. METHOD OF CFD ANALYSIS

2.1 Outline of Mini-Channel Model

Figure 1 shows a schematic of a calculation model of the mini-channel investigated in this study. This calculation model simulates the water-cooled mini-channel in miniaturized water cooling devices found in electronic equipment. The dimensions of the model was normalized by the mini-channel height d_d. The mini-channel length was 25 d_d, and its height was d_d. The rib was mounted 10 d_d behind the inlet of the mini-channel to enhance heat transfer. The rib width was 1/2 d_d. The rib height δ_r was varied between $\delta_r/d_d = 0.1$ and $\delta_r/d_d = 0.8$ to evaluate the effect of the rib height on the heat transfer performance of the pulsating flow. For comparison, an analysis of the flow without the rib (hereinafter called "$\delta_r/d_d = 0.0$") was additionally conducted. The working fluid was water.

The heat was generated from the bottom of the flow passage to simulate the heat generation of electrical chips. The heat transfer performance on the bottom of the channel was evaluated in the range of

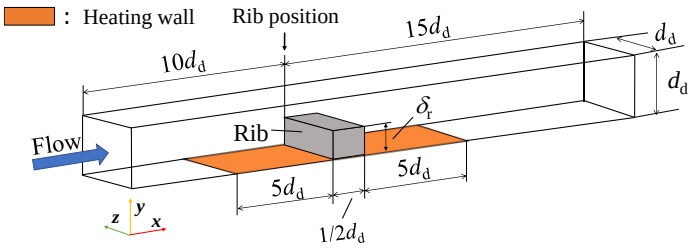

(a) Dimensions of CFD analysis model

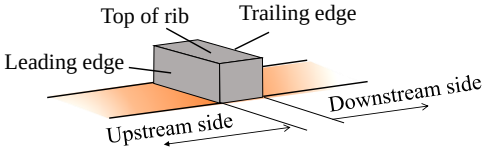

(b) Name of each surface.

Fig. 1 Schematic of CFD analysis model

5 times the mini-channel height (5 d_d) at both upstream and downstream of the rib.

The governing equations were the equation of continuity, the Navier-Stokes equation, and the energy equation (The Open CAE Society of Japan, 2016). They are shown below.

(a) Equation of Continuity

$$\left(\nabla \cdot \vec{u}\right) = 0 \tag{1}$$

(b) Navier-Stokes Equation

$$\frac{\partial \vec{u}}{\partial t} + \nabla \cdot \left(\vec{u}\,\vec{u}\right) = -\nabla P + \nu \nabla^2 \vec{u} \tag{2}$$

(c) Energy Equation

$$\frac{\partial T}{\partial t} + \nabla \cdot \left(T\,\vec{u}\right) = \nabla \cdot \left(\alpha \nabla T\right) \tag{3}$$

where $\vec{u}$ [m/s] is velocity vector, t [s] is time, P [m^2/s^2] is static pressure divided by reference density, ν [m^2/s] is kinematic viscosity, T [K] is temperature and α [m^2/s] is thermal diffusivity.

2.2 Conditions of CFD Analysis

Table 1 shows the conditions of the CFD analysis. Transient CFD analysis was performed from the initial condition to the quasi-steady state. Figure 2 shows the condition of the pulsating waveform. The shape of the waveform was a trapezoidal wave close to the square wave. The waveform was the same as in our previous paper (Hiratsuka et al., 2020). The waveform acceleration period was 0.5 sec. And the deceleration period was 0.5 sec. For comparison, steady flow analysis was also conducted in which the time-averaged flow rate was the same as the pulsating flow (hereafter called "0 Hz"). The following Reynolds number was determined using the time-averaged flow velocity. The relationship between the inertial force and the fluid flow's viscous force was used to decide the time-averaged supply flow rate condition.

Global Digital Central
ISSN: 2151-8629

$$Re = \frac{u_d d_e}{\nu} \quad (4)$$

where u_d [m/s] is the time-averaged flow velocity in the channel, and d_e [m] is the hydraulic diameter in the channel. To evaluate the effects of the pulsating flow in the lower supply flow rate condition observed in narrow cooling channels, the time-averaged Reynolds number was set between 10 and 600.

Figure 3 shows the boundary conditions of the proposed model. Figure 3(a) shows the boundary conditions of the velocity. In the case of the steady flow, the inlet velocity was set to a constant. On the other hand, in the pulsating flow, the inlet velocity was changed periodically. All the walls were treated as no-slip walls. Figure 3 (b) shows the boundary conditions of the pressure field. The inlet boundary and each wall boundary were constant pressure gradients and the outlet boundary was constant pressure. Figure 3 (c) shows the boundary conditions of the temperature field. The inlet boundary was the constant temperature. The other walls were treated as the thermal insulation boundary. The surface of the rib was represented as the insulation. We aimed to evaluate the level of heat transfer enhancement by the rib on the heating surface of the mini-channel. Therefore the heat transfer in the rib itself was not considered. The uniform heat flux condition was set on the heating surface, and the heat was generated into the channel.

The mesh number of the model was about 2,000,000. The mesh number was decided by the preliminary calculation, in which the relationship between the mesh number and the calculation result was evaluated. Table 2 shows the conditions of the mesh resolution evaluation of the proposed calculation model. As the preliminary calculation, a relationship between the time-averaged temperature rise distribution on the heating area behind the test rib (rib height = 1/2 d_d) and the mesh resolution under the pulsating flow condition in the case of Re = 500. Figure 4 shows the difference in the temperature rise distribution. The temperature distribution of Model 2 shows excellent agreement with Model 1, which has the most significant mesh number. Therefore, we accepted Model 2 as the mesh resolution of the proposed calculation model. Practically, to reduce the calculation cost, the mesh

Table 1 Conditions of CFD Analysis

Flow condition	Laminar
Working fluid	Water
Reynolds number	10, 20, 40, 100, 200, 400, 600
Frequency	1 Hz, 0 Hz (Steady)
Mesh number	2,072,000 ~ 2,084,000
Ratio of rib height and channel height δ_r/d_d	0.0, 0.1, 0.2, 0.5, 0.8

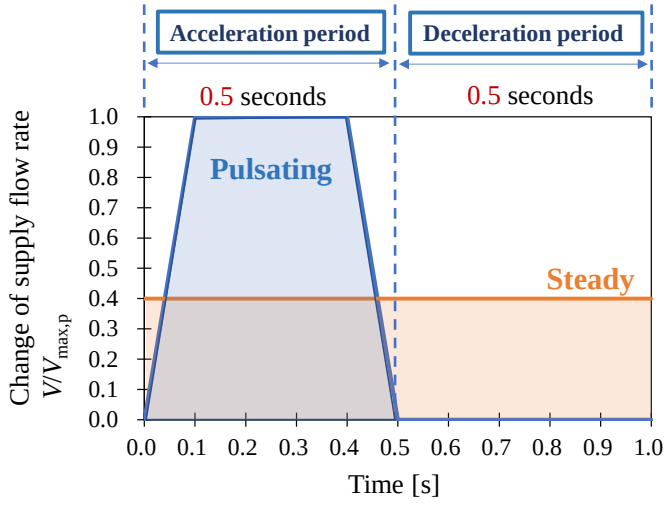

Fig. 2 Condition of pulsating waveform

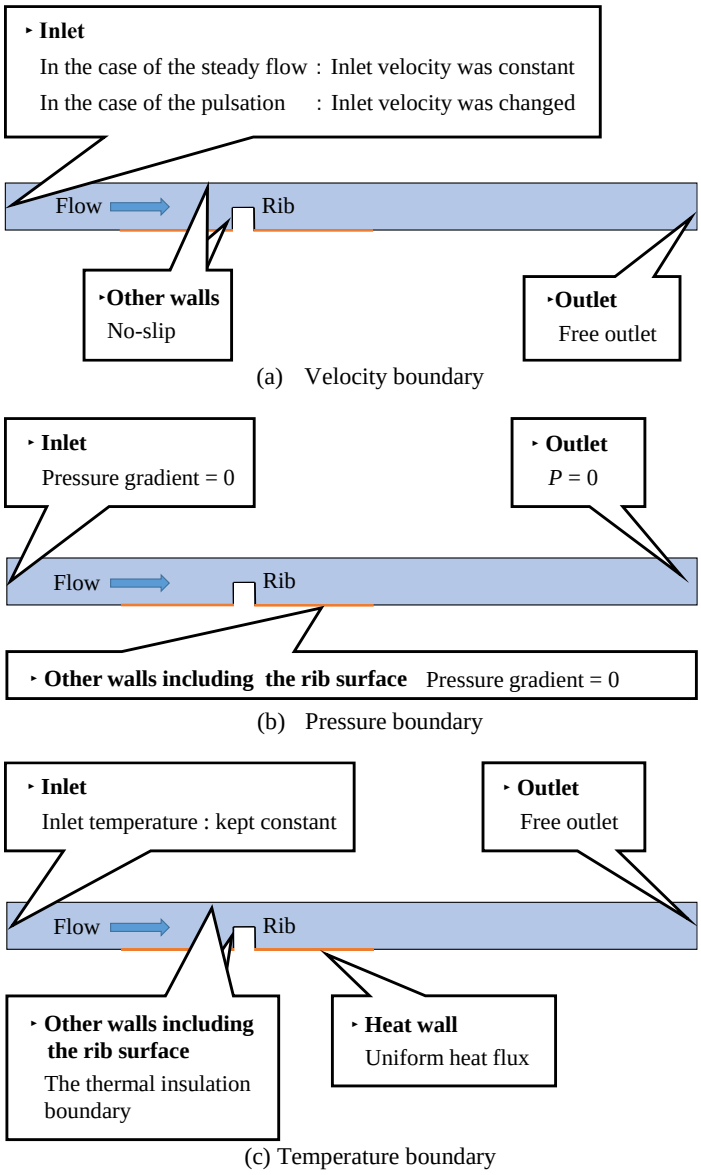

Fig. 3 Boundary conditions of each calculation model

Table 2 Conditions of mesh resolution investigation

Mesh condition	Mesh numbers
Model 1	3548716
Model 2 (accepted)	2326900
Model 3	974700
Model 4	495468

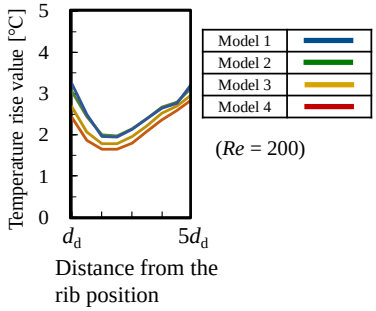

Fig. 4 Relationship between mesh resolution and time-averaged temperature distribution on the heating surface behind rib by pulsating flow

Global Digital Central
ISSN: 2151-8629

resolution near the output boundary in the investigated model, in which the effects of the mesh resolution on the flow and heat transfer characteristic around the rib become small, was decreased, and we optimized the calculation cost. Therefore, the final mesh number of the proposed model became about 2,000,000. About the time division, the time step of 1 cycle was automatically controlled during the calculation to keep the maximum Courant number below 0.5.

2.3 Evaluation Method of Heat Transfer Performance

The change of the heat transfer coefficient of the pulsating flow was evaluated by Nusselt number, pressure drop characteristic, and flow visualization. The local Nusselt number Nu_x and the average Nusselt number Nu_m are expressed as follows:

$$Nu_x = \frac{h_x \cdot 2d_e}{\lambda} \tag{5}$$

$$Nu_m = \frac{1}{A}\int_A Nu_x dA \tag{6}$$

where λ [W/(m·K)] is the thermal conductivity of water, and A [m^2] is the heat transfer area of the heating surface of the mini-channel. The characteristic length of the Nusselt number was defined as twice the height of the flow passage. The local Nusselt number was evaluated every $1/2d_d$ in the flow direction, as shown in Fig. 5. The local heat transfer coefficient h_x [W/(m^2·K)] was evaluated by the following equation:

$$h_x = \frac{q}{T_{\text{wall},x} - T_{\text{fluid}}} \tag{7}$$

where q [W/m^2] is heat flux from the bottom surface, $T_{\text{wall},x}$ [K] is the local temperature on the bottom surface, and T_{fluid} [K] is the inlet temperature of the water.

On the other hand, the pressure drop was also evaluated. The cooling performance index η was calculated to evaluate the improvement of the heat transfer performance of the pulsating flow against the steady flow (Webb and Eckert, 1972).

$$\eta = \frac{St_p / St_s}{\left(f_p / f_s\right)^{\frac{1}{3}}} \tag{8}$$

where St (= Nu/(Re/Pr)) is Stanton number and Pr is Prandtl number. The subscript p indicates the value of the pulsating flow, and the subscript s indicates the value of the steady flow without rib. f is Fanning's friction factor and is defined as follows:

$$f = \frac{\Delta P d_e}{\rho u_d^2 l} \tag{9}$$

where ρ [kg/m^3] is the water density, l [m] is the flow passage length, and ΔP [Pa] is the pressure drop. ΔP was obtained from the static pressure difference between the position $2d_d$ rear the inlet boundary and $2d_d$ before the outlet boundary.

Results of the proposed analysis were evaluated by the time-averaged value as shown in the following formulas.

$$Re_{(time-averaged)} = \frac{1}{t}\int_t Re dt \tag{10}$$

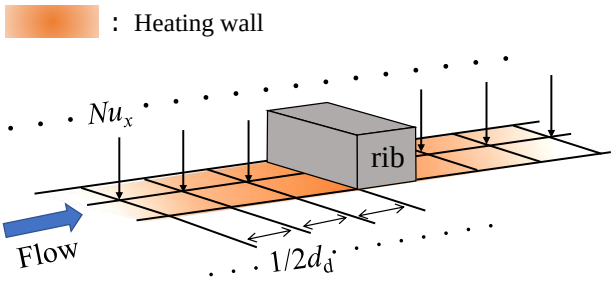

Fig. 5 Evaluation position of the local Nusselt number

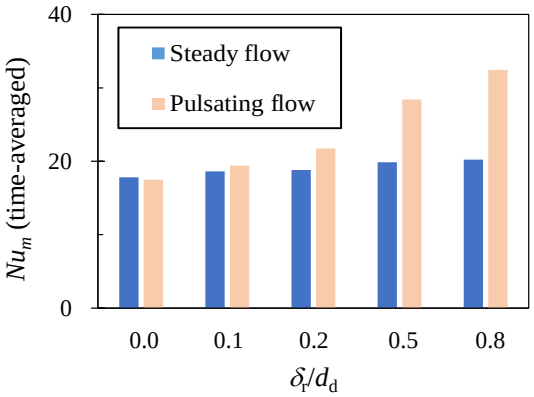

Fig. 6 Comparison of time-averaged Nu_m on the heating surface with the rib between steady flow and pulsating flow (Re = 200)

$$Nu_{x(time-averaged)} = \frac{1}{t}\int_t Nu_x dt \tag{11}$$

$$Nu_{m(time-averaged)} = \frac{1}{t}\int_t Nu_m dt \tag{12}$$

$$f_{(time-averaged)} = \frac{1}{t}\int_t f dt \tag{13}$$

$$\eta_{(time-averaged)} = \frac{1}{t}\int_t \eta dt \tag{14}$$

3. RESULTS OF CFD ANALYSIS

3.1 Nusselt Number

Figure 6 shows the change of the time-averaged Nu_m in the case of Re = 200. We can see that the average Nusselt number of the pulsating flow became higher than that of the steady flow regardless of its height. On the other hand, the level of heat transfer enhancement by the pulsating flow depended on the rib height. When the rib height became higher, a higher heat transfer coefficient was confirmed.

Figures 7 through 9 show the relationship between the distance from the rib and the time-averaged Nu_x of the steady flow and the pulsating flow at various Reynolds numbers. Figure 7 shows the results for δ_r/d_d = 0.2; Fig. 8, for δ_r/d_d = 0.5; and Fig. 9, for δ_r/d_d = 0.8. The horizontal axis is the distance from the rib, and the dotted line is the rib position, as shown in Fig. 1. The time-averaged Nu_x became higher as the time-averaged Reynolds number became higher regardless of the existence of the flow pulsation. Additionally, the time-averaged Nu_x became higher in the pulsating flow than in the steady flow. In particular, on the downstream side, the time-averaged Nu_x by the pulsating flow showed a higher heat transfer coefficient against the steady flow. In addition, the

Global Digital Central
ISSN: 2151-8629

peak value of the time-averaged Nu_x and the peak position were dependent on the time-averaged Reynolds number and the rib height. When the rib height became higher, the time-averaged Nu_x was enhanced. However, the peak heat transfer coefficient position moved to the downstream side of the channel. The results demonstrated that the rib and the pulsating flow could enhance heat transfer. On the other hand, the level of heat transfer enhancement by the pulsating flow was dependent on the rib height and the Reynolds number.

Time-transient change of the averaged Nusselt number on the heating surface with the rib in the case of Re = 200 was denoted in Fig. 10. We can confirm that the transient change of the heat transfer was confirmed according to the change of the pulsating motion.

3.2 Flow Visualization

We also investigate a relationship between the flow pattern around the rib and the heat transfer enhancement. Figure 11 shows the velocity distribution on the x–y cross-section at the center of the z-direction. Figure 12 demonstrates the velocity distribution on the x–z cross-section at the middle of each rib height. The flow patterns for δ_r/d_d = 0.5 and δ_r/d_d = 0.8 are denoted. The steady flow patterns, the acceleration period of the pulsating flow, and the deceleration period of the pulsating flow are denoted, respectively.

To begin with, the results for the steady flow indicated that flow separation at the rear of the rib appeared regardless of the Reynolds number and the rib height. However, the area of the flow separation area was changed by the Reynolds number and the rib height. From comparing the distribution of the time-averaged Nu_x with the flow pattern, the heat transfer decreased in the flow separation area. The position of the peak heat transfer became closer to the reattachment point of the main flow. From Fig. 8, in the case of Re = 600 and δ_r/d_d = 0.5, the peak point of the time-averaged Nu_x cannot be confirmed. In the case of δ_r/d_d = 0.8, a similar tendency can also be confirmed when the Reynolds number exceeds 200. In these cases, the reattachment point of the main flow cannot be observed on the surface of the heating area. Therefore, the unique peak point of the heat transfer coefficient was not caused.

On the other hand, when pulsating, the flow separation area and the reattachment point's position were changed against the steady flow. In practice, during the acceleration period of the pulsating flow, the position of the reattachment point moved from the near the rib to the downstream side of the channel according to the acceleration of the flow.

This change of flow stirred the flow behind the rib. During the acceleration period, the generation of the vortices was observed behind the rib. In addition, during the deceleration period, the mixing of the water between the main flow and the rear of the rib was confirmed regardless of the rib height. When the rib height became higher or the Reynolds number became higher, the peak velocity of the generated flow behind the rib during the deceleration period became faster, and the structure of the flow pattern became complex.

From these results of the flow visualization, we can conclude that the generation of the flow pulsation can stir the flow behind the rib during both the acceleration period and the deceleration period. The generation of the additional flow by the pulsation enhances the mixing of the water between the main flow and the rear of the rib. This enhances the heat transfer around the rib. The level of the mixing is dependent on the rib height and the Reynolds number.

Here, the heat transfer performance in front of the rib was enhanced against the steady flow when pulsating. This was caused by the increase in the peak velocity of the flow when pulsating. In this study, when the time-averaged Reynolds number is the same, the peak flow velocity of the pulsating flow is higher than the steady flow, as shown in Fig. 2. Significantly during the acceleration period, the fast flow impinges to the leading edge of the rib and enhances heat transfer in front of the rib. The difference in the peak flow velocity also enhances heat transfer in front of the rib against the steady flow.

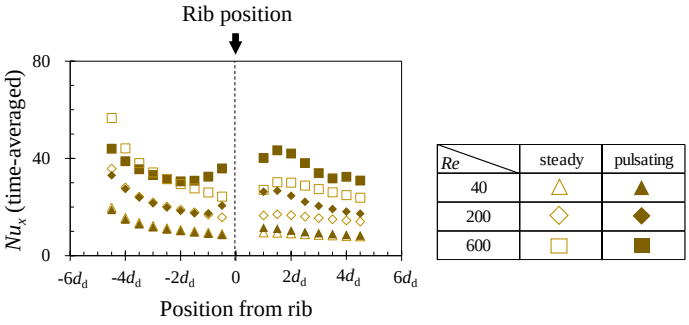

Fig. 7 Distribution of time-averaged Nu_x on heating surface with rib when pulsating (δ_r/d_d = 0.2)

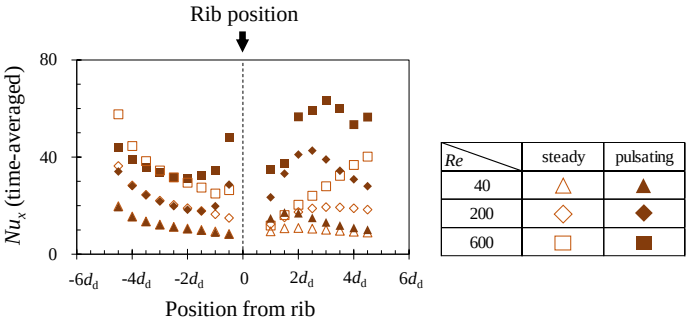

Fig. 8 Distribution of local Nusselt number on heating surface with rib when pulsating (δ_r/d_d = 0.5)

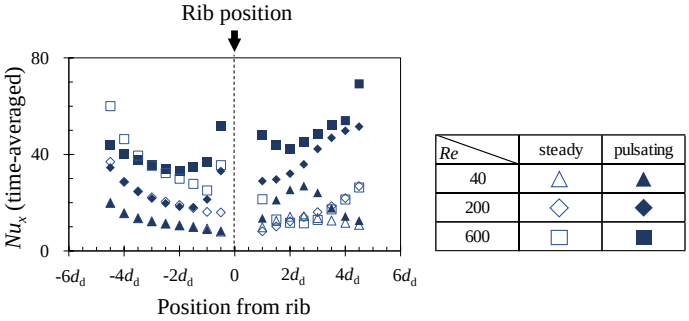

Fig. 9 Distribution of local Nusselt number on heating surface with rib when pulsating (δ_r/d_d = 0.8)

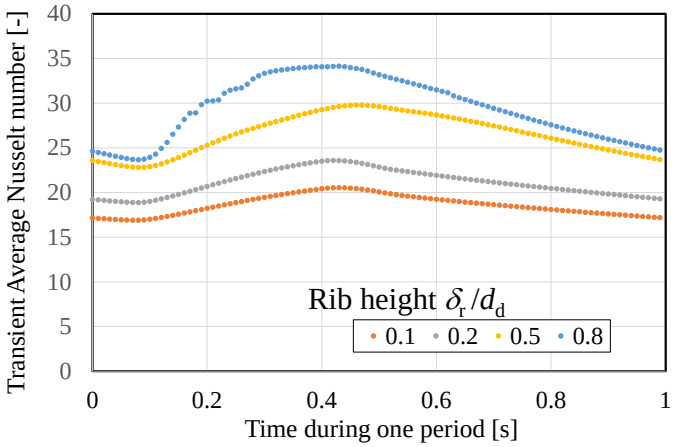

Fig. 10 Time-transient change of the averaged Nusselt number during one period (Re = 200).

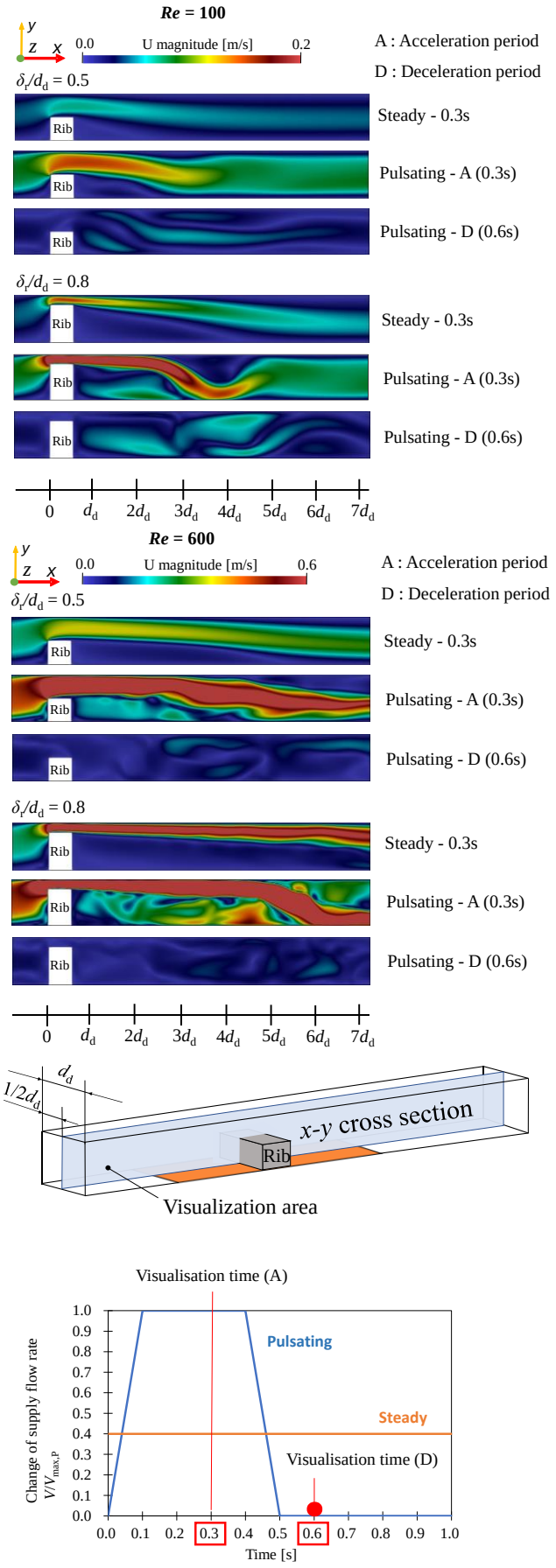

Fig. 11 Flow pattern differences between steady flow and pulsating flow (*x-y* cross-section)

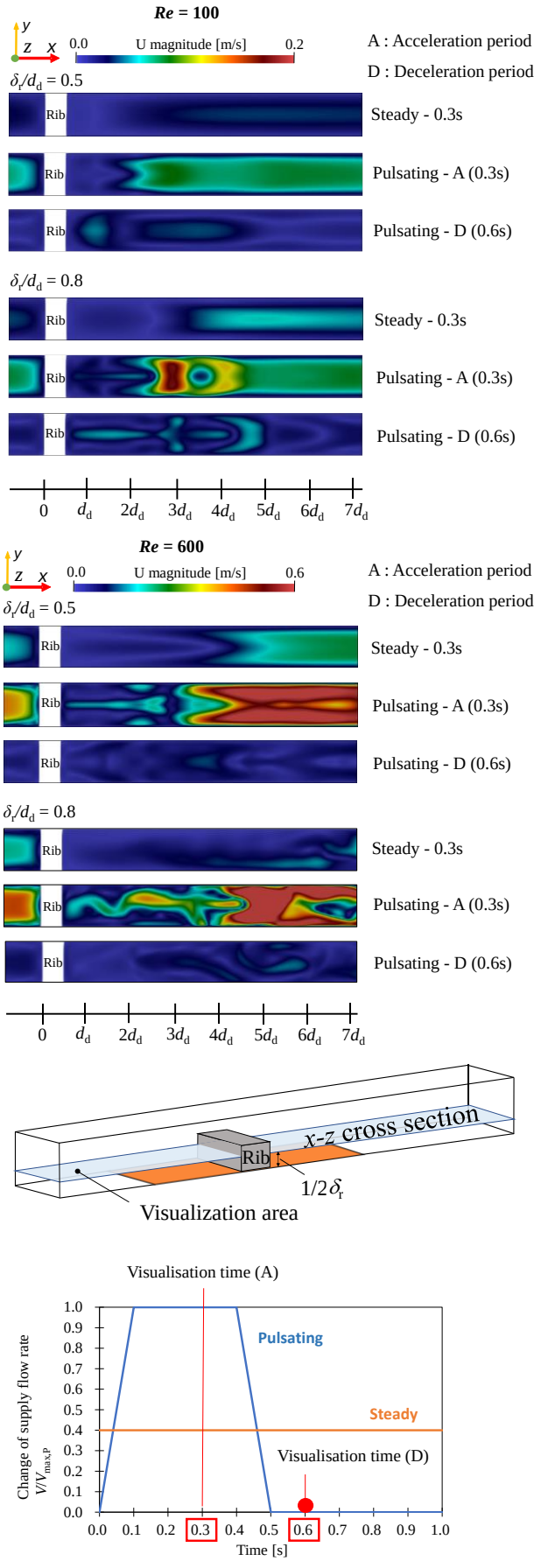

Fig. 12 Flow pattern differences between steady flow and pulsating flow (*x-z* cross-section)

Global Digital Central
ISSN: 2151-8629

3.3 Cooling Performance Index

We discuss the whole cooling performance around the rib. Hereafter, we discuss the heat transfer and the pressure drop characteristics by using the time-averaged values.

Figure 13 shows a relationship between Reynolds number and the average Nusselt number on the heating surface at various rib heights. Figure 14 shows the relationship between Reynolds number and change of pressure drop at various rib heights. Here, results was normalized by the result of the steady flow. Therefore, when $Nu_{m,p}/Nu_{m,s}$ is higher than 1.0, the average Nusselt number of the pulsating flow becomes higher than that of the steady flow experiment when the time-averaged supply flow rate is the same.

This result indicated that the level of heat transfer enhancement was dependent on the rib height. On the other hand, the pressure drop increased with the Reynolds number, and this tendency was confirmed regardless of the rib height. In particular, the increase of the pressure drop became significant because of the narrow clearance in the case of δ_r/d_d = 0.8. Therefore, the higher rib height can enhance heat transfer by the pulsating flow; however, the pressure drop also increases.

In order to evaluate the optimum rib height from the viewpoint of both the heat transfer and the pressure drop, we discuss the relationship between the cooling performance index η (defined as Eq. (8)) and the rib height. Figure 15 shows the relationship between η and the Reynolds number. When η becomes higher than 1, we can judge that the level of the heat transfer enhancement is higher than the level of the increase of the pressure drop. In the case of δ_r/d_d = 0.1, 0.2, and 0.5, η was higher than 1 regardless of the time-averaged Reynolds number. In these cases, we can conclude that enough heat transfer performance against the pressure drop increase is achieved. In contrast, the decrease of η was observed in the case of δ_r/d_d = 0.8. This is attributed to the significant pressure drop increase relative to the increase of the heat transfer performance. Therefore, from the viewpoint of the increase of the heat transfer performance of the combination of the pulsating flow and the rib, while inhibiting net power consumption of the pumps, a design of an optimum fin height against the Reynolds number should be conducted.

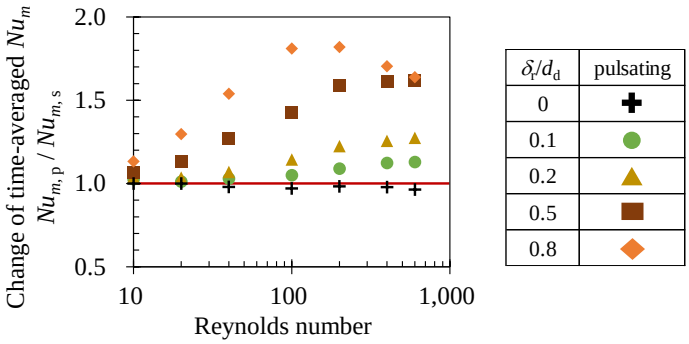

Fig. 13 Comparison of average Nusselt number between steady flow and the pulsating flow

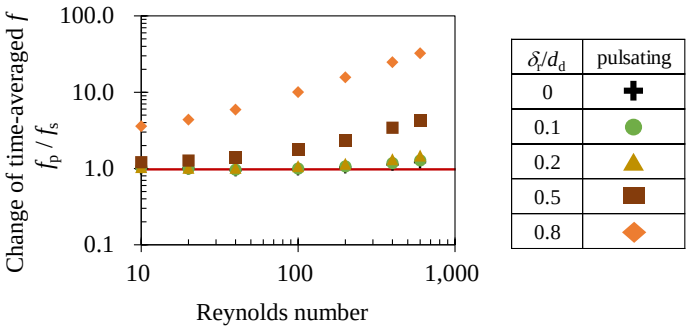

Fig. 14 Comparison of pressure drop between the steady flow and the pulsating flow

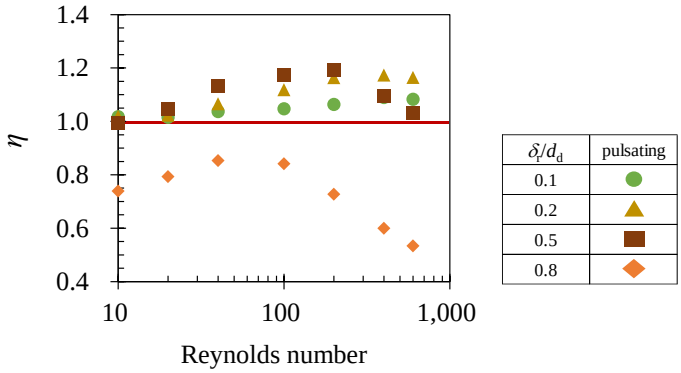

Fig. 15 Relationship between Reynolds number and η when rib was mounted on channel

4. CONCLUSIONS

In order to enhance the heat transfer in the narrow water cooling channel in the miniaturized cooling devices, we investigated the relationship between the heat transfer performance of the pulsating flow and the height of the rib mounted in the water channel through three- dimensional CFD analysis. Through the investigation, we draw the following conclusions:

The heat transfer enhancement by the pulsating flow can be confirmed regardless of the rib height. The level of the heat transfer enhancement is dependent on the rib height. This is caused by the flow pattern change around the rib by the generation of the pulsating flow.

The pressure drop characteristic becomes higher due to the pulsating flow generation and the higher rib height. When thermal cooling is made much necessary, the higher rib height is suitable. When the pressure drop is taken into consideration, the optimal rib height that promotes the heat transfer by the pulsating flow is changed by the Reynolds number. From the viewpoint of the cooling performance index, a design method of an optimum fin height should be developed against the pulsating flow condition. Future research will discuss a rib design guideline to optimize the heat transfer performance while controlling the pressure drop.

ACKNOWLEDGEMENTS

This work was supported by JSPS KAKENHI Grant Numbers JP16K18022, JP19K04249, and JP19K14916.

NOMENCLATURE

A	heat transfer area on bottom surface of mini-channel (m^2)
b	width (mm)
d	diameter (m)
f	Fanning's friction factor (Time-averaged) (-)
g	acceleration due to gravity (m/s^2)
h	rib height (mm)
h_x	heat transfer coefficient ($W/(m^2 \cdot K)$)
l	flow passage length (m)
Nu	time-averaged Nusselt number (-)
P	static pressure divided by reference density (m^2/s^2)
Pr	Prandtl number (-)
q	heat flux (W/m^2)

Re	Reynolds number (-)
St	Stanton number (-)
T	temperature (K)
t	time (s)
u	velocity (m/s)
V	flow rate (m^3/s)

Greek Symbols

α	thermal diffusivity (m^2/s)
ΔP	pressure drop (Pa)
δ	height (m)
η	cooling performance index (-)
λ	thermal conductivity (W/(m·K))
ν	kinematic viscosity of water (m^2/s)
ρ	water density (kg/m^3)

Subscripts

d	channel
e	hydraulic value in mini-channel
fluid	fluid
m	average
max	maximum value
p	pulsating flow
r	rib
s	steady flow
wall	bottom surface
x	local
0	reference

REFERENCES

Bons, J. P., Sondergaard, R. and River, R. B., 2000, "Turbine Separation Control Using Pulsed Vortex Generator Jets", *Journal of Turbomachinery*, **123**(2), 198-206.
https://doi.org/10.1115/1.1350410

Boonloi, A. and Jedsadaratanachai, W., 2022, "Effects of Blockage Locations for Enhanced Heat Trasnfer and Flow Visualizaiton in a Tested Duct located with Dual-Inclined Baffle (DIB): A CFD Analysis", *Frontiers in Heat and Mass Trasnfer*, **18**(19).
http://dx.doi.org/10.5098/hmt.18.19

Davletshin, L. A., Mikheev, A. N., Mikheev, N. I. and Shakirov. R. R., 2020, "Heat Transfer ad Structure of Pulsating Flow behind a Rib", *International Journal of Heat and Mass Transfer*, **160**, 120173.
https://doi.org/10.1016/j.ijheatmasstransfer.2020.120173

Ebrahimi, A., Rikhtegar, F., Sabaghan, A. and Roohi, E., 2016, "Heat transfer and entropy generation in a microchannel with longitudinal vortex generators using nanofluids", *International Journal of Energy*, **101**, 190-201.
https://doi.org/10.1016/j.energy.2016.01.102

Ebrahimi, A., Naranjani, B., Milani, S. and Javan, F. D., 2017, "Laminar convective heat transfer of shear-thinning liquids in rectangular channels with longitudinal vortex generators", *Journal of Chemical Engineering Science*, **173**, 264-274.
https://doi.org/10.1016/j.ces.2017.07.044

Fiebig, M., Valencia, A. and Mitra, N. K., 1993, "Basic Study on Flow and Heat Transfer Performance of Pulsating Air Flow for Application to Electronics Cooling", *Journal of Experimental Thermal and Fluid Science*, **7**(4), 287-295.
https://doi.org/10.1016/0894-1777(93)90052-K

Fukue, T., Hirose, K., and Yatsu, N., 2014, "Basic Study on Flow and Heat Transfer Performance of Pulsating Air Flow for Application to Electronics Cooling", *Transactions of the Japan Institute of Electronics Packaging*, **7**.
https://doi.org/10.5104/jiepeng.7.123

Gongnan, X., Shian, L., Bengt, S. and Weihong, Z., 2014, "Dynamics for thermal performance of a water-cooled minichannel heat sink with different chip arrangements", *International Journal of Numerical Methods for Heat & Fluid Flow*, **24**(4).
https://doi.org/10.1108/HFF-01-2013-0013

Hiratsuka, W., Fukue, T., Shirakawa, H., Nakayama, K. and Koito, Y., 2020, "CFD-BASED STUDY ON HEAT TRANSFER ENHANCEMENT BEHIND A PROJECTION IN A MINIATURIZED FLOW CHANNEL BY PULSATING FLOW", *Frontiers in Heat and Mass Transfer*, **15-16**.
http://dx.doi.org/10.5098/hmt.15.16

Miura, T., Matsubara, K. and Sakurai, A., 2011, "Spatially Developing DNS of Turbulent Heat Transfer in a Channel with Ribs Probing Heat Transfer Enhancement Mechanisms (in Japanese)". *Transactions of the Japan Society of Mechanical Engineers series B*, **78**.

Mochizuki, S., Murata, A. and Saito, H., 2007, "Axial Heat Transport Mechanism due to Reciprocating Flow in a Ribbed Tube (in Japanese)", *Transactions of the Japan Society of Mechanical Engineers series B*, **73**, 276-282.

Morikita Publishing Co., Ltd., Japan, 2016, "Numerical Analysis of Heat Transfer and Fluid Flow by OpenFOAM (in Japanese) ", The Open CAE Society of Japan, ISBN: 4627691017.

Obata, K., Fukue, T., Hirose. K., Kikuchi, M., Ueda, Y., Kusabuka, S. and Miyahara, T., "Enhancement of Water-Cooling Performance in Narrow Flow Passages by Using Micro Heat Sinks with Miniature Vortex Generators", *Proceedings of ASME InterPACK2015*, **1**.
https://doi.org/10.1115/IPACK2015-48607

Singh, R., Lapp, G., Velardo, J., Long, P. T., Mochizuki, M., Akbarzadeh, A., Date, A., Mausolf, K. and Busse, K., 2021, "Battery Cooling Options in Electric Vehicles with Heat Pipes", *Frontiers in Heat and Mass Trasnfer*, **16**(2).
http://dx.doi.org/10.5098/hmt.16.2

Saha, P. and Biswas, G., 2011, "NUMERICAL SIMULATION OF TURBULENT FLOW IN A RECTANGULAR CHANNEL WITH PERIODICALLY MOUNTED LONGITUDINAL VORTEX GENERATORS", *Frontiers in Heat and Mass Transfer*, **2**.
http://dx.doi.org/10.5098/hmt.v2.3.3008

Sakai, T., 2010, Department of Systematic Nursing Specialized Basic, Human Body Structure and Function (1), Anatomical Physiology (in Japanese), *Igaku Shoin Ltd*., 158.

Shukla, A., Chaube, A., Gupta, S. and Sirsath, A., 2014, "EXPERIMENTAL INVESTIGATION ON HEAT TRANSFER AND FRICTION FACTOR CHARACTERISTICS OF A STATIONARY SQUARE DUCT ROUGHENED BY V AND A-SHAPED RIBS", *Frontiers in Heat and Mass Transfer*, **5-14**.
http://dx.doi.org/10.5098/hmt.5.14

Scholl, S., Verstraete, T., Douchaine, F. and Gicquel, L., 2016, "Conjugate heat transfer of a rib-roughened internal turbine blade cooling channel using large eddy simulation", *International Journal of Heat and Fluid Flow*, **62**, 650-664.
https://doi.org/10.1016/j.ijheatfluidflow.2016.07.009

Takahashi, T., Watanabe, K. and Sakai, T., 2007, "Conjugate Heat Transfer Calculation of a Gas Turbine Rotor Blade with Ribbed Internal Cooling Passages (in Japanese)", *Transactions of the Japan Society of Mechanical Engineers, series B*, **73**, 161-166.

Valrdo, J., Singh, R., Ahamed, M. S., Mochizuki, M., Date, A. and Akbarzadeh, A., 2021, "Thin Thermal Management Modules using Flattened Heat Pipes and Piezoelectric Fans for Electronic Devices",

Global Digital Central
ISSN: 2151-8629

Frontiers in Heat and Mass Trasnfer, **17**(1).
http://dx.doi.org/10.5098/hmt.17.1

Webb, L. and Eckert, E. R. G., 1972, "APPLICATION OF ROUGH SURFACES TO HEAT ECCHANGER DESIGN", *International Journal of Heat Mass Transfer*, **15**, 1647-1658.

Weilin, Q. and Mudawar, I., 2002, "Experimental and numerical study of pressure drop and heat transfer in a single-phase micro-channel heat sink", *International Journal of Heat and Mass Transfer*, **45**(12), 2549-2565.
https://doi.org/10.1016/S0017-9310(01)00337-4

Wu, J. M. and Tao, W. Q., 2008, "Numerical study on laminar convection heat transfer in a rectangular channel with longitudinal vortex generator. Part A: Verification of field synergy principle", *International Journal of Heat and Mass Transfer*, **51**(5-6).
https://doi.org/10.1016/j.ijheatmasstransfer.2007.03.032

Yabo, W., Kai, Z., Zhuo, C., Hailong, L. and Jie, W., 2019, "Evaluation of Water Cooling Heat Sink Performance and Dynamic Flow Effect", *Journal of Energy Procedia*, **158,** 2417-2422.
https://doi.org/10.1016/j.egypro.2019.01.294

Yang, B., Gao, T., Gong, J. and Li, J., 2018, "Numerical investigation on flow and heat transfer of pulsating flow in various ribbed channels", *Journal of Applied Thermal Engineering*, **145**, 576-589.
https://doi.org/10.1016/j.applthermaleng.2018.09.041